JGR Solid Earth

RESEARCH ARTICLE
10.1029/2023JB027731

Earth's "Missing" Chlorine May Be in the Core

Liang Yuan[1,2] and **Gerd Steinle-Neumann**[2]

[1]State Key Laboratory of Geological Processes and Mineral Resources, and School of Earth Sciences, China University of Geosciences, Wuhan, China, [2]Bayerisches Geoinstitut, Universität Bayreuth, Bayreuth, Germany

Key Points:

- Using quantum mechanical calculations, we find that chlorine changes behavior from lithophile to siderophile in the deep Earth
- Fluorine, on the other hand, remains strongly lithophile for all pressure–temperature conditions relevant to planetary core formation
- Earth's superchondritic fluorine/chlorine ratio can plausibly be explained by chlorine sequestration into the core

Supporting Information:

Supporting Information may be found in the online version of this article.

Correspondence to:

L. Yuan,
yuanliang@cug.edu.cn;
liang.yuan@uni-bayreuth.de

Citation:

Yuan, L., & Steinle-Neumann, G. (2024). Earth's "missing" chlorine may be in the core. *Journal of Geophysical Research: Solid Earth*, *129*, e2023JB027731. https://doi.org/10.1029/2023JB027731

Received 24 AUG 2023
Accepted 28 JAN 2024
Corrected 2 APR 2024

This article was corrected on 2 APR 2024. See the end of the full text for details.

Author Contributions:

Conceptualization: Liang Yuan, Gerd Steinle-Neumann
Data curation: Liang Yuan
Funding acquisition: Liang Yuan, Gerd Steinle-Neumann
Investigation: Liang Yuan, Gerd Steinle-Neumann
Methodology: Liang Yuan, Gerd Steinle-Neumann
Supervision: Gerd Steinle-Neumann
Writing – original draft: Liang Yuan
Writing – review & editing: Gerd Steinle-Neumann

Abstract The budget of volatile halogens in the bulk silicate Earth, fluorine and chlorine, differs distinctly from that of chondritic meteorites. Arguably, the bulk silicate Earth shows a low abundance of Cl, while the F budget is in line with the expected volatility trend. One hypothesis for the missing Cl is its sequestration into Earth's core during planetary segregation, but experimental data on partitioning between silicate and metallic melts are limited in pressure and remain inconclusive. Here we use computational quantum mechanical methods to study F and Cl geochemistry during core–mantle differentiation over a wide pressure and temperature range. Our calculations reveal that with increasing pressure and temperature, chlorine shows an enhanced affinity for iron metal. The Cl metal–silicate partition coefficient $\log_{10}D_{\mathrm{Cl}}^{\mathrm{m/s}}$ increase from -1.89 ± 0.84 at 10 GPa and 3000 K to 1.62 ± 0.80 at 130 GPa and 5000 K, while corresponding calculations for F show minimal variations in metal–silicate partitioning across the pressure–temperature conditions investigated, yielding $\log_{10}D_{\mathrm{F}}^{\mathrm{m/s}}$ values between -3.61 ± 0.81 and -3.37 ± 0.80. The shift in $\log_{10}D_{\mathrm{Cl}}^{\mathrm{m/s}}$ shows a transition from lithophile to siderophile behavior. Further calculations on isotopic partitioning show negligible fractionation of Cl isotopes ($^{37}\mathrm{Cl}/^{35}\mathrm{Cl}$) between the mantle and core. Our results suggest that metallic iron within Earth's mantle and core may serve as an important Cl reservoir, potentially accounting for up to 40% of Earth's overall Cl inventory.

Plain Language Summary Chlorine plays a critical role within Earth's systems: balancing cellular charge and osmotic potential; regulating ocean salinity; transporting ore-forming metal in geological fluids; degrading stratospheric ozone. Despite its importance, the amount of chlorine in the planet has been poorly understood due to uncertainty in the composition of Earth's core, likely the largest reservoir that contains most of the Earth's volatile elements, for example, hydrogen and carbon. Here, we demonstrate that chlorine becomes increasingly compatible with metal compared to silicate at pressure–temperature conditions at which Earth's core formed. Conversely, fluorine as another halogen element continues to show a strong affinity for rocks. Therefore, substantial amounts of chlorine may exist within the Earth's core.

1. Introduction

A significant portion of the volatiles forming the atmosphere is believed to have originated from magmatic degassing from Earth's interior (Lammer et al., 2018), including halogens like fluorine (F) and chlorine (Cl) (Halmer et al., 2002). During volcanic activity, halogens are released from the mantle and can have substantial impact on Earth's climate and biodiversity. A notable example is the Cretaceous–Paleogene mass extinction associated with the volcanic eruptions leading to the Deccan Traps: The release of toxic gases, particularly chlorine and sulfur, has been proposed to result in catastrophic climate effects and ultimately extinction of three-quarters of life on Earth including dinosaurs (Glišović & Forte, 2017; Green et al., 2022; Self et al., 2008). It is thus of great interest to understand Earth's halogen budget and cycle.

The abundance and distribution of halogens within terrestrial reservoirs are influenced by various processes, including the delivery, retention, and loss of volatiles during Earth's formation (Hirschmann, 2016). In general, Earth's mantle displays a depletion pattern of volatile elements that aligns with their condensation temperatures (T_{C}). As a result of low T_{C}, halogens are depleted in the mantle: Fluorine is depleted consistently with the volatility trend, but the abundance of heavier halogens like Cl is lower by an order of magnitude relative to the volatility trend (Lodders, 2003; McDonough & Sun, 1995; Palme & O'Neill, 2014). However, both the abundance of elements and their T_{C} have uncertainties. For example, Clay et al. (2017) determined the halogen contents in carbonaceous chondrites and suggested lower solar-system Cl abundances compared to earlier estimates (e.g., Palme & O'Neill, 2014), and Guo and Korenaga (2021) estimated higher halogen concentrations in the bulk silicate Earth (BSE). The former, in turn, has led to adjustments in the volatility of numerous elements (Wood et al., 2019) and a revised T_{C} of Cl that mitigates its depletion in Earth's mantle. However, subsequent work

(Lodders & Fegley, 2023; Palme & Zipfel, 2022) has highlighted potential analytical problems in Clay et al. (2017), leading to apparent low halogen concentrations.

Despite discrepancies in absolute halogen abundances in the solar system, the relative concentration between F and Cl (i.e., F/Cl elemental ratio) in the BSE remains greater than primitive chondrites. This has been recognized as a distinct characteristic of BSE composition and is commonly referred to as the "missing Cl problem" (Marty, 2012; McDonough & Sun, 1995; Sharp & Draper, 2013). The superchondritic F/Cl ratio in the BSE raises questions about the behavior of halogens during Earth's accretion and segregation, and—similar to the non-chondritic elemental ratios of carbon/hydrogen and carbon/nitrogen (Hirschmann, 2016; Marty, 2012) and nitrogen isotopic composition (Shi et al., 2022) on Earth—suggests a complex history of volatile accretion. One hypothesis proposes that the late accretion of volatile-rich materials, often referred to as the "late veneer," delivered Earth's volatiles just after the core had formed on a dry proto-Earth (Albarède, 2009; Z. Wang & Becker, 2013). Marty (2012) estimated that 2% of primitive carbonaceous chondritic material added to a dry proto-Earth during late accretion could explain terrestrial Cl abundance, while the BSE fluorine abundance, by contrast, would require a significantly higher late accretionary contribution of ∼17%.

The high F/Cl ratio may indicate a preferential loss of Cl compared to F in the BSE. With highly volatile species like HCl (Zolotov & Mironenko, 2007) and a lower T_C (Wood et al., 2019), Cl may have been unable to accumulate efficiently onto planetary bodies in the inner solar system. As halogens tend to strongly bind with fluids that accumulate on the Earth's surface, another hypothesis suggests that Cl-rich near-surface reservoirs (the crust, oceans, and atmosphere) may have experienced evaporation losses due to collisional erosion (Sharp & Draper, 2013). However, in both scenarios, the removal of Cl from the BSE should also lead to the loss of a substantial amount of F. A third hypothesis is Cl sequestration into the core (McDonough & Sun, 1995). High pressure (P) and temperature (T) experiments (Kuwahara et al., 2017; Sharp & Draper, 2013) on Cl partitioning between iron and silicate liquids, however, suggest that Cl remains lithophile up to ∼23 GPa, making Earth's core an unlikely Cl reservoir, but a recent study (Yang et al., 2023) extended the experiments to show that both P and the presence of oxygen in the metal enhances the affinity of Cl for metallic environments, reaching siderophile behavior.

There are questions regarding the experimental work that prevent a definitive conclusion. First, experiments were performed using multi-anvil presses with limitations on the range of P–T; available experimental data on Cl partitioning is restricted to moderate P–T conditions below 23 GPa and 2700 K (Kuwahara et al., 2017; Mungall & Brenan, 2003; Sharp & Draper, 2013; Steenstra et al., 2020; Yang et al., 2023). However, core–mantle segregation, defining the equilibrium conditions for metal–silicate interactions, likely occurred at much higher $P \sim 50$ GPa and T exceeding 3500 K (Siebert et al., 2012). Determining the distribution of Cl in a deep magma ocean therefore requires significant extrapolation of experimental data, with associated uncertainty. Second, quenching silicate melt to glass becomes increasingly difficult as SiO_2 content decreases, P increases and volatile content rises (Bondar et al., 2020). Multi-anvil experiments conducted on pyrolite or peridotite compositions—chemically representative for the terrestrial magma ocean—have shown that depolymerized silicate melts tend to crystallize instead of forming a glass at $P > 10$ GPa (Armstrong et al., 2019). During such a quench, volatiles in the silicate melt may exsolve and be lost due to crystallization (Demouchy et al., 2005), making it unlikely that recovered crystalline samples represent the volatile content of the melt. Third, halogen elements are inherently vulnerable to loss during sample preparation; polishing metal samples recovered from high P–T experiments using oil- or water-based wetting agents can significantly decrease halogen concentrations due to their strongly hydrophilic nature, sometimes by an order of magnitude (Steenstra et al., 2020). Finally, when evaluating the accretion history of Earth's volatiles, the relative abundances of F and Cl may be equally, if not more important than their absolute concentrations. However, previous experiments have focused on the partitioning of Cl between metals and silicates. The limited availability of experimental data for F can be attributed, at least in part, to the considerable challenges involved in analyzing light halogens (Jennings et al., 2019).

To determine if core formation has resulted in a higher F/Cl ratio in the Earth's mantle compared to chondrites, it is essential to simultaneously examine their partitioning behavior between metal and silicate melts. Moreover, Earth's core is believed to host a substantial amount of primordial materials that likely account for geochemical anomalies such as high $^3He/^4He$ (Porcelli & Halliday, 2001) and low $^{182}W/^{184}W$ (Mundl-Petermeier et al., 2017) isotopic ratios in volcanic hotspots. To verify whether the core preserves halogens that potentially contribute to the distinctly low $^{37}Cl/^{35}Cl$ isotopic signatures of the deep mantle (Bonifacie et al., 2008), it is necessary to

characterize the Cl isotopic fingerprints of the core. In this study, we perform extensive density functional theory-based molecular dynamics simulations on F and Cl partitioning between iron and enstatite liquids across a broad range of P and T (10–130 GPa and 3000–5000 K), covering the conditions relevant to core formation, yet difficult to access experimentally. Our computer simulations reveal that during core formation at high P and T, chlorine exhibits siderophile behavior, supporting the hypothesis by McDonough and Sun (1995) on Cl sequestration to Earth's core. Fluorine, by contrast, remains strongly lithophile over the entire P–T range examined. Consequently, the low abundance of chlorine and the superchondritic F/Cl ratio in BSE might result from sequestration of chlorine into the core. In addition, our calculations suggest little to no equilibrium chlorine isotopic fractions between the mantle and core.

2. Methods

2.1. Element Partitioning

We investigate the partitioning behavior of F and Cl between $MgSiO_3$ and Fe liquids using two-phase coexistence molecular dynamics (MD) simulations (Morris et al., 1994) based on density functional theory (DFT). Further, we conduct Gibbs energy calculations using a combination of DFT-MD and thermodynamic integration (Frenkel & Smit, 1996) as a complementary method to validate and quantify the two-phase simulation results.

The two-phase simulation method was originally applied to compute the melting T of materials (Alfè, 2003; Laio et al., 2000; Morris et al., 1994; Usui & Tsuchiya, 2010). Subsequently, it has been extended to study elemental partitioning (Yuan & Steinle-Neumann, 2020; Zhang & Yin, 2012). Here, we directly model element partitioning by mimicking experiments where iron and $MgSiO_3$ liquids are brought in direct contact within a simulation box. By monitoring the distribution of halogen atoms as the system reaches equilibrium, we can gain a semi-quantitative understanding of halogen partitioning.

The partition coefficient of a solute (solu)—$D^{m/s}_{solu}$, defined as the ratio of F or Cl mass fraction in two solvents, Fe metal (superscript m) and $MgSiO_3$ silicate (superscript s)—is quantitively determined by examining the chemical equilibrium,

$$\mu^{m}_{solu}\left(P,T,c^{m}_{solu}\right) = \mu^{s}_{solu}\left(P,T,c^{s}_{solu}\right), \tag{1}$$

where μ_{solu} and c_{solu} are the chemical potential and mole fraction of solute in the metallic Fe and silicate liquids. We focus on liquid solutions that have small amounts of F and Cl since they are trace elements that exist in very low concentrations at levels of a few tens of μg/g in the BSE (McDonough & Sun, 1995; Palme & O'Neill, 2014). In these systems, it is appropriate to assume that the solute follows Henry's law,

$$\mu_{solu} = \mu^{\dagger}_{solu} + k_B T \ln c_{solu}, \tag{2}$$

and the solvent (solv) obeys Raoult's law,

$$\mu_{solv} = \mu^{0}_{solv} + k_B T \ln(1 - c_{solu}). \tag{3}$$

$\mu^{\dagger}_{solu}$ in Equation 2 represents the chemical potential of the solute in a hypothetical solution of unit concentration, while μ^{0}_{solv} in Equation 3 is the chemical potential of the pure solvent. The Gibbs energy G of the solution can then be expressed as

$$\begin{aligned} G &= N_{solu}\mu_{solu} + N_{solv}\mu_{solv} \\ &= N\left[c_{solu}\mu_{solu} + (1 - c_{solu})\mu_{solv}\right] \\ &= N\{c_{solu}\left[\mu^{\dagger}_{solu} + k_B T \ln c_{solu}\right] \\ &+ (1 - c_{solu})\left[\mu^{0}_{solv} + k_B T \ln(1 - c_{solu})\right]\}, \end{aligned} \tag{4}$$

where N_{solu} and N_{solv} are the number of formula units of solutes and solvents, respectively, and $N = N_{solu} + N_{solv}$. With G calculated at two solute concentrations using thermodynamic integration (Section 2.2), we can regress the

value of $\mu^{\dagger}_{\mathrm{solu}}$ (Equation 2); μ_{solu} can then be obtained for the silicate and metal separately. Finally, the equilibrium partition coefficient is calculated as $D^{\mathrm{m/s}}_{\mathrm{solu}} = \tilde{c}^{\mathrm{m}}_{\mathrm{solu}}/\tilde{c}^{\mathrm{s}}_{\mathrm{solu}}$, with mass concentrations $\tilde{c}$ converted from mole fraction c.

2.2. Gibbs Energy From Thermodynamic Integration

We evaluate the Gibbs energy of metal and silicate liquids, both with and without halogens, using a combination of thermodynamic integration (Frenkel & Smit, 1996) and DFT-MD. We conduct the thermodynamic integration from an ideal gas to a system controlled by DFT forces via the classical Weeks–Chandler–Andersen (WCA) fluid system (Supporting Information S1). In related work (Dorner et al., 2018; Taniuchi & Tsuchiya, 2018), a one-step thermodynamic integration was used, that is, directly from an ideal gas to a DFT state, eliminating the intermediate classical WCA system. However, simulating states close to the ideal gas limit within DFT can be challenging due to numerical instabilities caused by overlapping atom positions. As simulations are performed at constant V, the Helmholtz energy of the DFT system is then

$$F_{\mathrm{DFT}} = F_{\mathrm{IG}} + \Delta F_{\mathrm{IG}\rightarrow\mathrm{WCA}} + \Delta F_{\mathrm{WCA}\rightarrow\mathrm{DFT}}, \tag{5}$$

and G can be calculated by $G = F + PV$, with P from the DFT-MD trajectories. Details of thermodynamic integration can be found in Supporting Information S1.

2.3. Density Functional Theory Calculations

Electronic structure calculations based on Kohn–Sham DFT are performed using the VASP code (Kresse & Furthmüller, 1996) with a plane wave approach and periodic boundary conditions. Projector augmented wave-type pseudopotentials (Kresse & Joubert, 1999) are used with the Perdew-Burke-Ernzerhof generalized gradient approximation to the exchange-correlation functional (Perdew et al., 1996). DFT-MD simulations are performed in the *NVT* ensemble (i.e., at a constant number of particles N, volume V, and temperature T). These simulations are conducted for a minimum duration of 20 ps, using a time step of 1.0 fs. Electronic excitations at finite T are taken into account by using Fermi–Dirac smearing (Mermin, 1965). In two-phase coexistence MD simulations (Section 2.1) which require large system sizes (~350 atoms) and run for long time scales (up to 160 ps), we calculate the electronic Kohn–Sham DFT states using a single Γ point and a plane-wave energy cutoff of 450 eV. This set of cutoff and density of k-points balances acceptable accuracy with reasonable computational cost. For Gibbs energy calculations (Section 2.2), we instead use a $2 \times 2 \times 2$ Monkhorst–Pack k-mesh and a plane-wave energy cutoff of 800 eV. This ensures that the energy convergence is <1 meV/atom. To effectively manage computational costs during the calculations, we use a two-step approach. We first use thermodynamic integration to determine the Helmholtz energy of the DFT system calculated on the Γ point and with an energy cutoff of 400 eV ($\mathrm{DFT}_{\Gamma,\ 400}$). Then, we perform additional thermodynamic integration from $\mathrm{DFT}_{\Gamma,\ 400}$ to a $\mathrm{DFT}_{2\mathrm{k},\ 800}$ system with a $2 \times 2 \times 2$ Monkhorst-Pack k-mesh and an energy cutoff of 800 eV.

3. Results

3.1. Two-Phase Simulations of Element Partitioning

The starting configurations for two-phase coexistence MD simulations are prepared by equilibrating a metal (Fe_{150}) and a silicate ($Mg_{35}Si_{35}O_{105}$) cell under desired P–T conditions, each of them containing an equal number ($N = 9$) of Cl (F) atoms. These two cells are then merged into a slab and allowed to freely evolve under fixed *NVT* conditions. At high T, the silicate and metal liquids tend to mix, making it challenging to determine the distribution of halogen elements between the two phases. To overcome this issue, we choose a simulation T at which $MgSiO_3$ is supercooled but remains liquid. This minimizes mixing between the two phases and thus reduces statistical uncertainties in the time-evolution profiles in Figure 1. We investigate three compositional sets: (a) Cl-bearing systems, (b) F-bearing systems, and (c) Cl- and F-bearing systems. The simulations are conducted under two conditions: (a) low P–T with ~10 GPa and ~3000 K, and (b) high P–T with ~120 GPa and ~3800 K.

By examining the time evolution of Cl distribution, we find preferential migration of Cl from the metal to the silicate phase at the low P–T condition (10 GPa and 3000 K; Figure 1a, left panel). Between 0 and 30 ps, the number of Cl atoms in the metal gradually decreases to $N^{\mathrm{m}}_{\mathrm{Cl}} \sim 1$, while simultaneously, the number of Cl atoms in

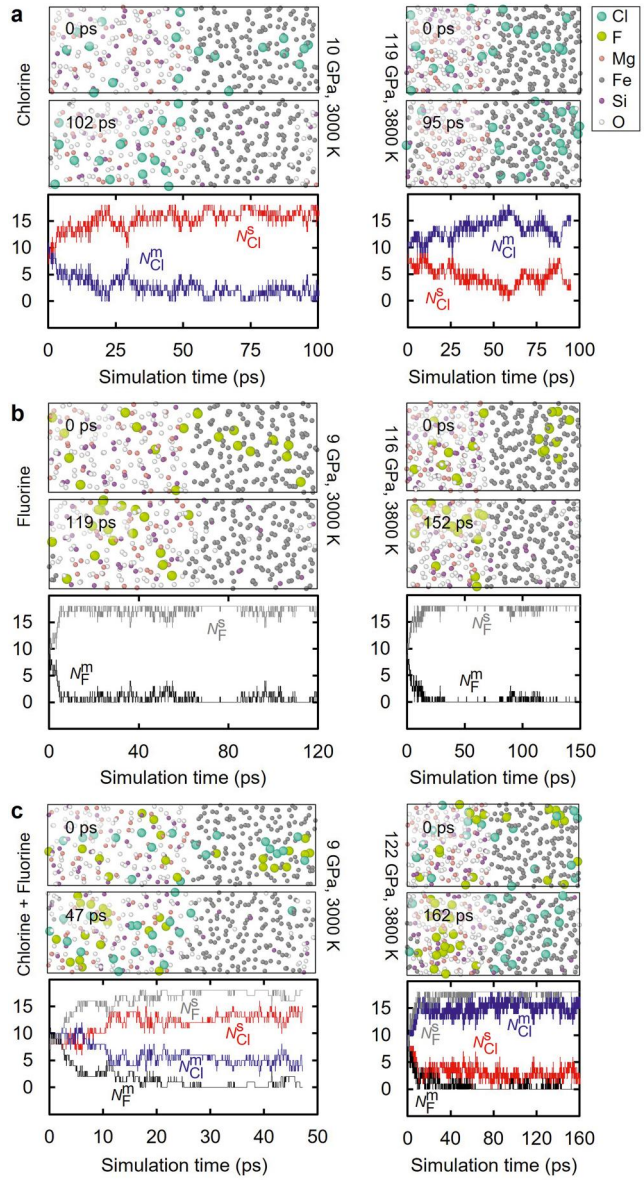

Figure 1. Results from two-phase DFT-MD simulation of chlorine (Cl) and fluorine (F) metal–silicate partitioning. (a) Initial and final snapshots (upper panels) for the Cl-bearing system and time-evolution (lower panel) of the number of Cl atoms in the silicate N^{s}_{Cl} and metallic N^{m}_{Cl} liquids for $Fe_{150}Cl_9$–$Mg_{35}Si_{35}O_{105}Cl_9$ at low pressure–temperature condition (10 GPa and 3000 K; left) and high pressure–temperature condition (119 GPa and 3800 K; right). (b) Initial and final snapshots (upper panels) for the F-bearing system and time-evolution (lower panel) of the number of F atoms in the silicate N^{s}_{F} and metallic N^{m}_{F} liquids for $Fe_{150}F_9$–$Mg_{35}Si_{35}O_{105}F_9$ at low pressure–temperature condition (9 GPa and 3000 K; left) and high pressure–temperature condition (116 GPa and 3800 K; right). (c) Initial and final snapshots (upper panels) for the F- and Cl-bearing system and time-evolution (lower panel) of the number of Cl (F) atoms in the silicate N^{s}_{Cl} (N^{s}_{F}) and metallic N^{m}_{Cl} (N^{m}_{F}) liquids for $Fe_{150}Cl_9F_9$–$Mg_{35}Si_{35}O_{105}Cl_9F_9$ at low pressure–temperature condition (9 GPa and 3000 K; left) and high pressure–temperature condition (122 GPa and 3800 K; right). The width of the left (low pressure) and right columns (high pressure) correspond to the relative sizes of the simulation cells.

the silicate increases to $N^{s}_{Cl} \sim 17$, suggesting that Cl exhibits higher compatibility with silicate compared to metal at low P–T conditions. The observed behavior is consistent with previous experimental results (Kuwahara et al., 2017; Sharp & Draper, 2013) and the generally accepted understanding of Cl as a lithophile element.

At the elevated P–T condition (120 GPa and 3800 K; Figure 1a, right panel), contrary to the prevailing view that Cl is lithophile, our simulations reveal a strong affinity of Cl for iron. This is demonstrated by preferential

migration of Cl from the silicate to the metal phase. Over a time span of 60 ps, N^{s}_{Cl} gradually decreases to ∼3, while N^{m}_{Cl} simultaneously increases to ∼15. Subsequently, the time evolution profiles of N^{s}_{Cl} and N^{m}_{Cl} exhibit fluctuations, which can be attributed to two factors: (a) frequent exchange of Cl between the two phases, and (b) statistical errors arising from challenges in accurately identifying the interface between the phases. These results provide evidence that, under *P–T* conditions relevant to the deep lower mantle, chlorine undergoes a transformation to a siderophile element.

By contrast, the results for fluorine consistently demonstrate that F partitions into the silicate phase rather than the metal at both *P–T* conditions (Figure 1b). The concentrations of F in the silicate approach $N^{s}_{F} \sim 18$ and in the metal $N^{m}_{F} \sim 0$ at $t = 10$ ps, and the fluctuations in $N^{s\,(m)}_{F}$ in Figure 1b are smaller compared to those of $N^{s\,(m)}_{Cl}$ in Figure 1a once the concentrations of F in the two phases reach equilibrium, indicating a stronger partitioning of F over Cl.

To ensure consistent *P–T* conditions in the two-phase simulations for Cl and F (Figure 1a vs. Figure 1b), we tried to iteratively refine the dimensions of the simulation boxes. However, the large number of atoms adds significant computational overhead to DFT and the search for appropriate cell sizes becomes a time-consuming trial-and-error process. Rather, we conduct a third set of simulations (Figure 1c) that include both F and Cl in the same simulation box, enabling us to directly compare their partitioning under identical *P–T* conditions. Like the results from the first two sets of simulations, we observe that both F and Cl exhibit a preference for migrating from the metal phase to the silicate phase at low *P–T* conditions (∼10 GPa and ∼3000 K), but F exhibits a higher degree of transfer compared to Cl with $N^{s}_{F} \sim 18$ versus $N^{s}_{Cl} \sim 13$ as the system approaches equilibrium. Also consistent with the individual two-phase simulations, we observe smaller fluctuations in the time evolution profiles for N^{s}_{F} and N^{m}_{F} compared to N^{s}_{Cl} and N^{m}_{Cl}. These results confirm the previously observed stronger lithophile behavior of F relative to Cl in the systems containing only one halogen species. Furthermore, we find that in the slab containing both F and Cl, the equilibrium concentration of Cl in the silicate phase is lower compared to that in the F-free, Cl-bearing system, with $N^{s}_{Cl} \sim 17$ in Figure 1a (left panel) versus $N^{s}_{Cl} \sim 13$ in Figure 1c (left panel). This finding suggests that the presence of F limits the solubility of Cl, indicating that these two elements may be mutually exclusive in silicate melt, at least at high concentrations.

At *P–T* conditions of 120 GPa and 3800 K (Figure 1c, right panel), fluorine shows lithophile characteristics by preferentially migrating from the metallic to the silicate phase, while Cl behaves as a siderophile element, moving in the opposite direction, supporting the observations from the first two sets of simulations (Figures 1a and 1b). A clear distinction between the two elements is also evident in the snapshot taken at the end of the simulation ($t = 162$ ps) when all Cl atoms reside in the metallic phase, and all F atoms reside in the silicate phase. The distinct separation of the two elements hints at their contrasting fate during metal–silicate equilibration in processes such as early core formation and present-day core–mantle interactions (Section 4.2).

In all two-phase simulations, we include concentrations of halogen atoms with $N^{m+s}_{Cl\ (or\ F)} = 18$ out of 343 total atoms in the cell and $N^{m+s}_{Cl+F} = 36/361$ that largely exceed levels found in natural magmas, aimed at increasing the frequency of halogen exchange between metal and silicate, thereby reducing the statistical fluctuations in the time evolution profiles. Despite high solute concentrations, our two-phase simulations consistently reveal the absence of clustering among halogen atoms in the silicate or metal melts as they approach equilibrium. This contrasts with noble gas–metallic iron systems, where such clustering via phase separation has been observed (Ostanin et al., 2006; Yuan & Steinle-Neumann, 2021). Therefore, even at high concentrations, halogens appear to remain within a dilute regime below the saturation point, allowing individual atoms—as opposed to clusters—to diffuse freely within the simulation box. The consistency of the results between the two-phase simulations and Gibbs energy calculations (Section 3.2) provides additional affirmation that the use of elevated solute concentrations does not significantly impact the results of two-phase simulations.

3.2. Gibbs Energy and Partition Coefficient

The partitioning behavior of Cl (F) between metal and silicate can be understood by considering the reaction Gibbs energy $\Delta_r G$ resulting from the exchange of a halogen atom between the two phases,

$$Mg_{15}Si_{15}O_{45} \cdot X + Fe_{75} \xrightarrow{\Delta_r G} Mg_{15}Si_{15}O_{45} + Fe_{75} \cdot X, \quad (6)$$

where X represents Cl (or F). When $\Delta_r G = \left(G_{Mg_{15}Si_{15}O_{45}} + G_{Fe_{75}\cdot X}\right) - \left(G_{Mg_{15}Si_{15}O_{45}\cdot X} + G_{Fe_{75}}\right)$ is positive (negative), it indicates a preference for the halogen atom to partition into silicate (metal). To confirm and quantify the results from two-phase simulations and gain an understanding of the thermodynamics involved in halogen metal–silicate partitioning, we calculate the Gibbs energies of all components in Equation 6 using thermodynamic integration (Section 2.2; Supporting Information S1) at four P–T conditions along a magma ocean isentrope (C. W. Thomas & Asimow, 2013): 10 GPa and 3000 K, 40 GPa and 4000 K, 80 GPa and 4500 K, and 130 GPa and 5000 K (Table S1 in Supporting Information S1).

Our calculations show that $\Delta_r G$ for Cl exchange reaction (Equation 6) is positive at low P–T conditions (10 GPa and 3000 K; Figure S1a in Supporting Information S1), indicating lithophile behavior. As we increase P and T to moderate conditions (40 GPa and 4000 K), $\Delta_r G$ approaches zero. At high P and T conditions (80 GPa and 4500 K, 130 GPa and 5000 K), $\Delta_r G$ becomes negative, indicating siderophile behavior. By contrast, F exchange yields large positive $\Delta_r G$ values across the entire P–T range considered (Figure S1c in Supporting Information S1), indicating a strong lithophile character. It is worth noting that a sign reversal of $\Delta_r G$ from negative to positive for Cl reflects a combined effect of both P and T as we adjust them simultaneously along potential magma ocean isentropes. To distinguish the effect of P from that of T, we break down $\Delta_r G$ into two terms: (a) a $P\Delta_r V$ term resulting from the difference between the partial molar volumes of Cl in metal ($\overline{V}^{m}_{Cl}$) and silicate ($\overline{V}^{s}_{Cl}$), and (b) the remaining contribution that accounts for internal energy and entropic effects. At $P = 10$ GPa and $T = 3000$ K, we observe $\overline{V}^{m}_{Cl} < \overline{V}^{s}_{Cl}$, with a relative difference of $\left(\overline{V}^{s}_{Cl} - \overline{V}^{m}_{Cl}\right)/\overline{V}^{s}_{Cl} \approx 15\%$. At $P = 130$ GPa and $T = 5000$ K, the difference increases to ~25%. The variation in $\Delta_r V$ has a significant impact on the effect of P on the change in $\Delta_r G$, as indicated by the consistent trend observed between $\Delta_r G$ and $P\Delta_r V$ (Figures S1a and S1b in Supporting Information S1). By contrast, $\overline{V}^{m}_{F} > \overline{V}^{s}_{F}$, but the difference $\left(\overline{V}^{m}_{F} - \overline{V}^{s}_{F}\right)/\overline{V}^{s}_{F}$ is small (~8%) at the condition of 130 GPa and 5000 K, leading to limited $P\Delta_r V$ effects (Figure S1d in Supporting Information S1). The primary driving force for F migration from metal to silicate comes from internal energy differences and entropic effects.

To calculate halogen metal–silicate partition coefficients, we obtain the values of $\mu^{\dagger}_{Cl}$ ($\mu^{\dagger}_{F}$) (Equation 4; Table S1 in Supporting Information S1) from the DFT-MD Gibbs energy results, that allow the determination of the concentration-dependent chemical potentials of Cl (F) in metal μ^{m}_{Cl} (μ^{m}_{F}) and silicate μ^{s}_{Cl} (μ^{s}_{F}) solutions (Equation 2; Figures 2a–2d): $\mu^{s}_{Cl} < \mu^{m}_{Cl}$ at 10 GPa, reflecting lithophile behavior; at higher P–T $\mu^{s}_{Cl} > \mu^{m}_{Cl}$, indicating siderophile behavior, consistent with the results from the two-phase simulations and the analysis of $\Delta_r G$. On the other hand, fluorine is consistently lithophile for all conditions considered, as μ^{s}_{F} is significantly smaller than μ^{m}_{F} across the explored P–T range. From the chemical potentials, the halogen metal–silicate partition coefficients $D^{m/s}_{Cl}$ ($D^{m/s}_{F}$) can be calculated using Equation 1 (Figure 2e): $\log_{10} D^{m/s}_{Cl}$ increases from -1.89 ± 0.84 at 10 GPa and 3000 K to 1.62 ± 0.80 at 130 GPa and 5000 K; for fluorine, there is no significant variation in $D^{m/s}_{F}$ with P–T, with $\log_{10} D^{m/s}_{F}$ ranging from -3.61 ± 0.81 to -3.37 ± 0.80.

3.3. Chlorine Isotope Fractionation

Previous experiments have shown that even at high T conditions there is a significant fractionation of isotopes of elements such as carbon (Satish-Kumar et al., 2011), nitrogen (Y. Li, Marty, et al., 2016; Shi et al., 2022), silicon (Shahar et al., 2009), and tin (Kubik et al., 2021) associated with core formation. This fractionation occurs due to the influence of mass differences on Gibbs energies in coexisting metal and silicate phases, and scales with $(m_h - m_l)/(m_h \cdot m_l)$ (Equation S8 in Supporting Information S1). It is therefore expected that metal–silicate equilibration may cause stronger fractionation of chlorine isotopes (^{35}Cl and ^{37}Cl) compared to heavier elements like tin.

To assess if the segregation of Earth's core and mantle leads to resolvable differences in Cl isotopes between these reservoirs, we conduct calculations to determine its equilibrium isotope fractionation factor (Equation S7 in Supporting Information S1) between metallic and silicate melts. We estimate the Cl isotope fractionation based on configurational snapshots extracted from MD trajectories for compositions $Fe_{75}Cl$ and $Mg_{15}Si_{15}O_{45}Cl$, equilibrated at 10 GPa and 3000 K. The force constants $k_{hf} = 48.92 \pm 1.15$ N/m acting on the Cl atom in the metal are larger than in the silicate with average $k_{hf} = 43.48 \pm 0.62$ N/m (Figures S2a and S2b in Supporting Information S1). The k_{hf} values translate to isotope fractionation factors $1{,}000 \cdot \ln\alpha^{m/s} < +0.01‰$ at $T > 3500$ K (Figure S2c in Supporting Information S1).

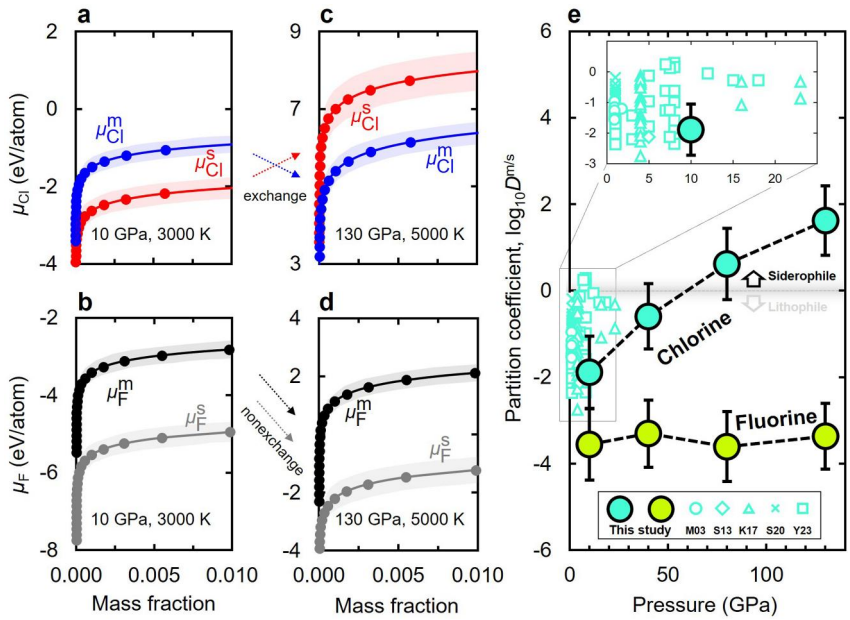

Figure 2. Chemical potentials μ and metal–silicate partition coefficients $D_{Cl}^{m/s}$ and $D_{F}^{m/s}$ for Cl and F. μ of Cl in silicate μ_{Cl}^{s} and in metal μ_{Cl}^{m} (a, c), and F in silicate μ_{F}^{s} and in metal μ_{F}^{m} (b, d) as a function of Cl (F) content, in mass fraction at low (a, b) versus high (c, d) pressure–temperature conditions. $D_{Cl}^{m/s}$ and $D_{F}^{m/s}$ (on a log scale) as a function of pressure determined by equal μ in each phase (e). Inset in panel (e): zoom-in on the low-pressure region showing our predicted $D_{Cl}^{m/s}$ in comparison with available experimental Cl partitioning data between metal (or sulfur-bearing metal) and silicate: Mungall and Brenan (2003) (M03: circles), Sharp and Draper (2013) (S13: diamond), Steenstra et al. (2020) (S20: circles), Yang et al. (2023) (Y23: squares). To the best of our knowledge, there have been no studies that explicitly document the metal–silicate partition coefficients for F.

Considering that $1{,}000{\cdot}\ln\alpha^{m/s}$ is insensitive to P (W. Wang et al., 2021; Yuan & Steinle-Neumann, 2022), our isotope fraction value implies that any equilibrium fractionation of Cl isotopes associated with core formation will go undetected within the analytical error range of ±0.14‰ in δ^{37}Cl measurements (e.g., Bonifacie et al., 2008). Despite considerable Cl isotope variations in terrestrial reservoirs with measured δ^{37}Cl ranging from −3 to 0‰ in mid-ocean ridge basalts (MORB) (Bonifacie et al., 2008; Layne et al., 2009; Sharp et al., 2007) and from −2 to +3‰ in oceanic island basalts (OIB) (John et al., 2010), the similarity in δ^{37}Cl between BSE and carbonaceous chondrites (Sharp et al., 2007) requires that there should be little to no fractionation between the mantle and core, supporting the extremely small $1{,}000{\cdot}\ln\alpha^{m/s}$ values predicted in this study.

4. Discussion

McDonough and Sun (1995) discussed the possibility that Cl might have been transported to the Earth's center during core formation, an idea that has not yet found convincing support. High P–T experiments indicate that Cl has limited solubility in iron metal and exhibits lithophile characteristics (Kuwahara et al., 2017; Mungall & Brenan, 2003; Sharp & Draper, 2013; Steenstra et al., 2020). Through extensive DFT calculations, we present evidence that supports the original concept by McDonough and Sun (1995). Our computational results align with recent high P–T experiments by Yang et al. (2023), indicating an transition in Cl partitioning behavior from lithophile to siderophile during core formation. With the predicted $D_{Cl}^{m/s}$, we find that a substantial amount of Cl might have been extracted from the silicate mantle, and the core could potentially account for ∼40% of Earth's Cl inventory (Section 4.2), challenging the prevalent notion that Cl is mainly concentrated in surface reservoirs. Fluorine, on the other hand, strongly partitions into silicate throughout the entire P–T range of core formation.

4.1. Comparison With Previous Studies

The partitioning of Cl between metal and silicate phases has been investigated by high P–T experiments (Kuwahara et al., 2017; Mungall & Brenan, 2003; Sharp & Draper, 2013; Steenstra et al., 2020; Yang et al., 2023),

with strongly differing results. Low $D_{Cl}^{m/s}$ by Kuwahara et al. (2019) and Sharp and Draper (2013), for example, may be influenced by Cl dissolution and/or redistribution during wet-polishing (Steenstra et al., 2020), as well as exposure to air (Yang et al., 2023). To minimize potential reactions with water and atmospheric moisture, the metal–silicate samples recovered from high P–T experiments by Yang et al. (2023) were polished dry and stored in a vacuum chamber prior to chemical analysis. Our predicted $D_{Cl}^{m/s}$ at 10 GPa and 3000 K falls within the range of existing experimental data (Figure 2e, inset), at the lower end of experimental $D_{Cl}^{m/s}$ (Yang et al., 2023). Yang et al. (2023) found that the partitioning of Cl to the metallic liquid increases with oxygen content. Therefore, it seems plausible that using iron–oxygen alloys, instead of the pure iron examined in this study, could further improve the agreement between $D_{Cl}^{m/s}$ predicted by DFT-MD and experimental determinations.

To the best of our knowledge, there have been no studies that explicitly determine the metal–silicate partition coefficients for fluorine. However, the experiments conducted by Steenstra et al. (2020) highlight two crucial observations that are consistent with our results: (a) negligible amounts of F partition into metal melt that coexists with silicate melt, below the detection limit of an electron probe micro analyzer; (b) there is a discernible trend wherein halogens, with increasing atomic radius, exhibit higher compatibility with metal, indicating $D_{F}^{m/s} < D_{Cl}^{m/s}$.

4.2. Earth's Cl and F Budgets

The partition coefficients we have predicted offer insights solely into the relative concentrations of Cl and F in metals and silicates as they achieve equilibrium. To estimate the absolute amount of Cl and F in the core, and consequently in the bulk Earth, we need to know halogen concentrations in the magma ocean, against which the core was equilibrated. Previous studies have estimated the Cl (F) budgets of the BSE indirectly, using reference elements in the MORB or OIB mantle source and elemental ratios that undergo minimal fractionation during mantle melting (e.g., F/K and Cl/Rb). The estimated halogen budgets for the BSE fall in the range of 17–30 μg/g for Cl and 25 μg/g for F (McDonough & Sun, 1995; Palme & O'Neill, 2014). Using an alternative scaling approach, Guo and Korenaga (2021) arrived at higher concentrations (81 μg/g for Cl and 57 μg/g for F). To estimate the Cl (F) budgets of Earth's core, we begin by considering a single-stage core formation model with equilibrium conditions of 50 GPa and 4000 K, representing a first-order approximation to a much more complicated and stochastic core formation process (Siebert et al., 2012). With $D_{Cl}^{m/s} \sim 0.5$ from our DFT predictions, and using values of 17–81 μg/g Cl in the BSE (Guo & Korenaga, 2021; McDonough & Sun, 1995; Palme & O'Neill, 2014), equilibration between metal and silicate results in a Cl concentration of 9–44 μg/g (equivalent to $1.77–8.42 \cdot 10^{19}$ kg) in the core. In either scenario, this corresponds to 20% of Earth's total Cl content. For fluorine, our calculations indicate an F budget of 0.01–0.02 μg/g ($1.59–3.62 \cdot 10^{16}$ kg), <0.1% of Earth's total F content.

Multistage core formation models (e.g., Rubie et al., 2011; Rudge et al., 2010; Wade & Wood, 2005) offer the advantage of addressing the evolving conditions of core–mantle differentiation along with a self-consistent evolution of oxygen fugacity (f_{O_2}). Unlike other volatile species, such as carbon (Y. Li, Dasgupta, et al., 2016), nitrogen (Shi et al., 2022) and sulfur (Boujibar et al., 2014) whose partitioning is notably affected by f_{O_2}, we expect an insignificant effect of f_{O_2} on Cl (F) partitioning (Section 4.3). Since we ignore the effects of f_{O_2} and use only pure Fe as the metal phase, and P and T are covaried in our DFT-MD simulations along potential magma ocean isentropes, we choose a second-order polynomial function of accretion P to fit the $\log_{10} D_{Cl\ (F)}^{m/s}$ results (Table S1 in Supporting Information S1). Using the parameterized $D_{Cl\ (F)}^{m/s}$, the concentrations of Cl (F) in the core and mantle are derived from (a) mass balance considerations and (b) partial core–mantle equilibrations in the accreting Earth following the approach of Rudge et al. (2010).

In each step of the multistage core formation modeling, we introduce a planetesimal (impactor) to interact with the proto-Earth (target): The impactor's entire mantle, a sizable portion (90%) of its core, and the mantle of the proto-Earth equilibrate, while the core of the proto-Earth remains undisturbed by the impacts. Within each step of this process, the equilibration of metal and silicate occurs under a constant fraction (0.6) of the growing P at the core–mantle boundary (CMB). P_{CMB} increases proportionally to mass accumulation (Turcotte & Schubert, 2002), with $P_{CMB} = 135$ GPa for the present-day Earth. The evolution of Cl concentration as a function of the accreted mass fraction of Earth is shown in Figure S3 in Supporting Information S1. We consider two sets of halogen compositions in the BSE provided by McDonough and Sun (1995) and Guo and Korenaga (2021). As Yang et al. (2023) used a Cl content for the bulk Earth of ~92 ppm, a value comparable to the BSE composition

proposed by Guo and Korenaga (2021), we compare their results with ours based on Guo and Korenaga (2021). In the extrapolation of the thermodynamic model for calculating Cl partition coefficients under magma ocean conditions, Yang et al. (2023) estimated $D_{\mathrm{Cl}}^{\mathrm{m/s}}$ to increase from 10^0 at 0 GPa to 10^6 at 80 GPa, in contrast to the increase from 10^{-2} to 10^2 in our study. This leads to two differences in predicted Cl distribution in the evolving Earth: (a) At low P or accreted mass fraction, our calculated Cl concentration in the core is lower than that reported by Yang et al. (2023), and (b) the decline in Cl in the BSE is more pronounced in Yang et al. (2023). Through multiple iterations aimed at matching the composition of the BSE (Guo & Korenaga, 2021; McDonough & Sun, 1995; Palme & O'Neill, 2014), we find 22–105 μg/g Cl in the core (i.e., 4.28–20.28 · 10^{19} kg, ~40% of Earth's total Cl content), larger concentrations than from the single-stage model. The resulting F content of the core is comparable to that derived from the single-stage model.

Given F and Cl concentrations of 25 μg/g and 17–30 μg/g, respectively, in the BSE, and 60 μg/g and 680 μg/g, respectively, in primitive chondrites (McDonough & Sun, 1995; Palme & O'Neill, 2014), we calculate the chondrite-normalized F/Cl ratio $R_{\mathrm{F/Cl}} = (\mathrm{F/Cl})_{\mathrm{BSE}}/(\mathrm{F/Cl})_{\mathrm{chondrite}}$ = 9–17. If chondrites and the Earth share the same F/Cl ratio, Earth's core needs to contain >90% of its Cl to reach $R_{\mathrm{F/Cl}} = 1$. The BSE halogen compositions from Guo and Korenaga (2021) (F = 57 μg/g and Cl = 81 μg/g) does not significantly alleviate the required Cl content in the core. On the other hand, using the updated chondritic Cl content of 110 μg/g (Clay et al., 2017), 55%–75% of Earth's Cl has to be in the core to achieve $R_{\mathrm{F/Cl}} = 1$. While the lower bound exceeds our highest estimate of 40%, it may fall within the range of uncertainty, considering error bars of $D_{\mathrm{Cl}}^{\mathrm{m/s}}$ and others effects, such as oxygen impurities in iron, that may increase $D_{\mathrm{Cl}}^{\mathrm{m/s}}$ as suggested by Yang et al. (2023).

4.3. Limitations, Complications, and Future Work

Although our DFT-MD results are generally consistent with previous experimental observations where available, it is important to highlight that the simulations provide constraints on the lithophile and siderophile characteristics of Cl and F in an idealized scenario with strongly simplified compositions of the magma ocean ($MgSiO_3$) and core (Fe). However, the Earth's core is not composed solely of pure iron; rather, it probably incorporates various light elements such as sulfur, silicon, oxygen, carbon, and hydrogen (Hirose et al., 2021). In recent experiments, Yang et al. (2023) have shown that oxygen, considered a candidate light element in the core, enhances partitioning of Cl into iron metals. On the other hand, some light elements, for example, silicon and sulfur (Kilburn & Wood, 1997), silicon and oxygen (Hirose et al., 2017), carbon and hydrogen (Hirose et al., 2019), have been observed to be mutually exclusive in iron metals. As a result, the collective impact of multiple impurities on $D_{\mathrm{Cl\ (F)}}^{\mathrm{m/s}}$ remains uncertain. Given the extremely high computational expense linked with sampling $D_{\mathrm{Cl\ (F)}}^{\mathrm{m/s}}$ extensively across the P–T–composition space relevant to the magma ocean, we vary P and T along a potential magma ocean adiabat to investigate their influence on partitioning; other factors, for example, f_{O_2}, are not considered. For Cl (F) partitioning, we expect an insignificant influence of f_{O_2}: unlike nitrogen that can exist in multiple oxidation states and its partitioning is therefore notably affected by f_{O_2} (Shi et al., 2022), the speciation of halogens remains largely unchanged as Cl^- (F^-) ions in both metal and silicate phases at different f_{O_2} (e.g., Thomas & Wood, 2021). Varying f_{O_2} in the MD simulations is complex (e.g., Cao et al., 2019), and in the context of modeling Earth materials, it has been, at best, approximated by varying the number of oxygen atoms rather than explicitly controlling oxygen partial pressure in the simulation cells. Examples are previous work on volatile dissolution/partitioning in silicate and metallic liquids at magma ocean conditions (e.g., Solomatova et al., 2019; Yuan & Steinle-Neumann, 2022). When estimating volatile element concentrations in the core through metal–silicate partitioning, the results strongly depend on mantle abundances and core formation scenarios. However, significant uncertainties are associated with both factors, as highlighted in Hirose et al. (2021). Additionally, planetary processes such as giant impact-induced degassing, mantle convection, slab subduction, and core–mantle interaction may have influenced BSE composition. Despite these considerations, quantifying their impact on Earth's halogen distribution and budget remains challenging. Nevertheless, the siderophile nature of Cl confirmed by both experiments (Yang et al., 2023) and our DFT-MD simulations support the possibility of the Earth's core serving as a significant reservoir for Cl.

Magma oceans may have only partially covered the mantle of the early Earth (J. Li & Agee, 1996; Siebert et al., 2012), implying that core-forming liquid metal had to permeate through a solid silicate matrix (Stevenson, 1990), understanding element partitioning in systems containing liquid metals and solid $MgSiO_3$ phases is

thus crucial. Despite substantial progress in MD methodology, conducting such studies poses considerable challenges. One major hurdle is the time-consuming process of sampling the configurational space of solids (Laio & Parrinello, 2002). This is mainly attributed to the extremely low probability of an atom crossing the energy barrier from one crystal lattice site to another due to the exponential decay of sampling probability with energy (Boltzmann distribution). To enhance configurational exploration, integrating the two-phase coexisting method with advanced sampling techniques holds significant potential, and there are various promising avenues to explore. One viable approach involves using methods such as hybrid Monte Carlo/MD sampling (Widom et al., 2014); however, implementing these techniques for computing element partitioning demands significant additional efforts.

To gain a better understanding of the halogen budget in the Earth's core, future work may focus on (a) measuring terrestrial planet and meteorite samples with improved analytical methods to address the current discrepancy in Cl abundance (Clay et al., 2017 vs. Lodders & Fegley, 2023), (b) expanding the experimental P ranges, (c) incorporating more complex structural (solid/liquid) and compositional atomistic models for the mantle (e.g., pyrolite) and core (i.e., multicomponent iron-based alloys) in DFT calculations, and (d) conducting geodynamical simulations that quantitatively address chemical exchange across the core–mantle boundary with Cl partitioning/diffusion results predicted at P_{CMB}. Such simulations, as demonstrated by Ferrick and Korenaga (2023) for helium and tungsten, can offer valuable insights into Earth's core contribution to halogen heterogeneities observed in the OIB mantle source (Waters, 2022).

5. Conclusions

Using DFT-MD simulations, we have conducted an extensive investigation into the partitioning behavior of chlorine and fluorine between metal and silicate phases under the extreme pressures and temperatures characteristic of core formation. Our calculations show that as pressure and temperature increase, chlorine exhibits an enhanced affinity for the metallic phase, marking a transition from lithophile to siderophile behavior at lower mantle pressure. To qualitatively illustrate this significant alteration, we have conducted two-phase simulations. To quantify the metal–silicate partition coefficients for chlorine ($D_{Cl}^{m/s}$) and fluorine ($D_{F}^{m/s}$), we have used a combination of density functional theory molecular dynamics and thermodynamic integration. For chlorine, $\log_{10}D_{Cl}^{m/s}$ increases from -1.89 ± 0.84 at 10 GPa and 3000 K to 1.62 ± 0.80 at 130 GPa and 5000 K. For fluorine, our calculations indicate negligible variation in the metal–silicate partition coefficient $\log_{10}D_{F}^{m/s}$ over the range of pressures and temperatures studied, with values ranging from -3.61 ± 0.81 to -3.37 ± 0.80. We have also calculated chlorine equilibrium isotope fractionation and found no discernible differences in chlorine isotope composition between coexisting metallic and silicate phases. Based on our results, we propose that the core and metallic iron present within the Earth's mantle (Frost et al., 2004) may serve as a substantial reservoir for chlorine, potentially accounting for up to 40% of the planet's overall chlorine inventory, accounting for the observed anomalous depletion of chlorine relative to fluorine within the mantle.

Data Availability Statement

Data related to this work, including scripts and simulation input files, are publicly available at Yuan (2023). Density functional theory calculations were performed using VASP which is proprietary software available for purchase (at https://www.vasp.at). Classical molecular dynamics simulations were performed with LAMMPS (https://www.lammps.org). Thermodynamic integration was performed using i-PI (https://ipi-code.org) interfaced with both VASP and LAMMPS.

Acknowledgments
This work was supported by the Deutsche Forschungsgemeinschaft (DFG, Grants STE1105/13-2 and YU358/1-1). L.Y. thanks the financial support from the Alexander von Humboldt Foundation, and the Fundamental Research Funds for the Central Universities, China University of Geosciences (Wuhan) (G1323523034). Computations were performed on resources provided by the Leibniz Supercomputing Center, and the research center for scientific computing at the University of Bayreuth. Comments by Yuan Li and an anonymous reviewer have significantly improved the manuscript. Open Access funding enabled and organized by Projekt DEAL.

References

Albarède, F. (2009). Volatile accretion history of the terrestrial planets and dynamic implications. *Nature*, *461*(7268), 1227–1233. https://doi.org/10.1038/nature08477

Alfè, D. (2003). First-principles simulations of direct coexistence of solid and liquid aluminum. *Physical Review B: Condensed Matter*, *68*(6), 064423. https://doi.org/10.1103/physrevb.68.064423

Armstrong, K., Frost, D. J., McCammon, C. A., Rubie, D. C., & Boffa Ballaran, T. (2019). Deep magma ocean formation set the oxidation state of Earth's mantle. *Science*, *365*(6456), 903–906. https://doi.org/10.1126/science.aax8376

Bondar, D., Fei, H., Withers, A. C., & Katsura, T. (2020). A rapid-quench technique for multi-anvil high-pressure-temperature experiments. *Review of Scientific Instruments*, *91*(6), 065105. https://doi.org/10.1063/5.0005936

Bonifacie, M., Jendrzejewski, N., Agrinier, P., Humler, E., Coleman, M., & Javoy, M. (2008). The chlorine isotope composition of earth's mantle. *Science*, *319*(5869), 1518–1520. https://doi.org/10.1126/science.1150988

Boujibar, A., Andrault, D., Bouhifd, M. A., Bolfan-Casanova, N., Devidal, J. L., & Trcera, N. (2014). Metal-silicate partitioning of sulphur, new experimental and thermodynamic constraints on planetary accretion. *Earth and Planetary Science Letters*, *391*, 42–54. https://doi.org/10.1016/j.epsl.2014.01.021

Cao, Y., Gadre, M. J., Ngo, A. T., Adler, S. B., & Morgan, D. D. (2019). Factors controlling surface oxygen exchange in oxides. *Nature Communications*, *10*(1), 1–15. https://doi.org/10.1038/s41467-019-08674-4

Clay, P. L., Burgess, R., Busemann, H., Ruzié-Hamilton, L., Joachim, B., Day, J. M. D., & Ballentine, C. J. (2017). Halogens in chondritic meteorites and terrestrial accretion. *Nature*, *551*(7682), 614–618. https://doi.org/10.1038/nature24625

Demouchy, S., Deloule, E., Frost, D. J., & Keppler, H. (2005). Pressure and temperature-dependence of water solubility in Fe-free wadsleyite. *American Mineralogist*, *90*(7), 1084–1091. https://doi.org/10.2138/am.2005.1751

Dorner, F., Sukurma, Z., Dellago, C., & Kresse, G. (2018). Melting Si: Beyond density functional theory. *Physical Review Letters*, *121*(19), 195701. https://doi.org/10.1103/physrevlett.121.195701

Ferrick, A. L., & Korenaga, J. (2023). Long-term core-mantle interaction explains W-He isotope heterogeneities. *Proceedings of the National Academy of Sciences of the United States of America*, *120*(4), e2215903120. https://doi.org/10.1073/pnas.2215903120

Frenkel, D., & Smit, B. (1996). *Understanding molecular simulation: From algorithms to applications*. Academic Press.

Frost, D. J., Liebske, C., Langenhorst, F., McCammon, C. A., Trønnes, R. G., & Rubie, D. C. (2004). Experimental evidence for the existence of iron-rich metal in the Earth's lower mantle. *Nature*, *428*(6981), 409–412. https://doi.org/10.1038/nature02413

Glišović, P., & Forte, A. M. (2017). On the deep-mantle origin of the Deccan Traps. *Science*, *355*(6325), 613–616. https://doi.org/10.1126/science.aah4390

Green, T., Renne, P. R., & Keller, C. B. (2022). Continental flood basalts drive Phanerozoic extinctions. *Proceedings of the National Academy of Sciences of the United States of America*, *119*(38), e2120441119. https://doi.org/10.1073/pnas.2120441119

Guo, M., & Korenaga, J. (2021). A halogen budget of the bulk silicate Earth points to a history of early halogen degassing followed by net regassing. *Proceedings of the National Academy of Sciences of the United States of America*, *118*(51), e2116083118. https://doi.org/10.1073/pnas.2116083118

Halmer, M. M., Schmincke, H. U., & Graf, H. F. (2002). The annual volcanic gas input into the atmosphere, in particular into the stratosphere: A global data set for the past 100 years. *Journal of Volcanology and Geothermal Research*, *115*(3–4), 511–528. https://doi.org/10.1016/s0377-0273(01)00318-3

Hirose, K., Morard, G., Sinmyo, R., Umemoto, K., Hernlund, J., Helffrich, G., & Labrosse, S. (2017). Crystallization of silicon dioxide and compositional evolution of the Earth's core. *Nature*, *543*(7643), 99–102. https://doi.org/10.1038/nature21367

Hirose, K., Tagawa, S., Kuwayama, Y., Sinmyo, R., Morard, G., Ohishi, Y., & Genda, H. (2019). Hydrogen limits carbon in liquid iron. *Geophysical Research Letters*, *46*(10), 5190–5197. https://doi.org/10.1029/2019gl082591

Hirose, K., Wood, B., & Vočadlo, L. (2021). Light elements in the Earth's core. *Nature Reviews Earth & Environment*, *2*(9), 645–658. https://doi.org/10.1038/s43017-021-00203-6

Hirschmann, M. M. (2016). Constraints on the early delivery and fractionation of Earth's major volatiles from C/H, C/N, and C/S ratios. *American Mineralogist*, *101*(3), 540–553. https://doi.org/10.2138/am-2016-5452

Jennings, E. S., Wade, J., Laurenz, V., & Petitgirard, S. (2019). Diamond anvil cell partitioning experiments for accretion and core formation: Testing the limitations of electron microprobe analysis. *Microscopy and Microanalysis*, *25*(1), 1–10. https://doi.org/10.1017/s1431927618015568

John, T., Layne, G. D., Haase, K. M., & Barnes, J. D. (2010). Chlorine isotope evidence for crustal recycling into the Earth's mantle. *Earth and Planetary Science Letters*, *298*(1–2), 175–182. https://doi.org/10.1016/j.epsl.2010.07.039

Kilburn, M. R., & Wood, B. J. (1997). Metal-silicate partitioning and the incompatibility of S and Si during core formation. *Earth and Planetary Science Letters*, *152*(1–4), 139–148. https://doi.org/10.1016/s0012-821x(97)00125-8

Kresse, G., & Furthmüller, J. (1996). Efficiency of ab-initio total energy calculations for metals and semiconductors using a plane-wave basis set. *Computational Materials Science*, *6*(1), 15–50. https://doi.org/10.1016/0927-0256(96)00008-0

Kresse, G., & Joubert, D. (1999). From ultrasoft pseudopotentials to the projector augmented-wave method. *Physical Review B: Condensed Matter*, *59*(3), 1758–1775. https://doi.org/10.1103/physrevb.59.1758

Kubik, E., Siebert, J., Mahan, B., Creech, J., Blanchard, I., Agranier, A., et al. (2021). Tracing Earth's volatile delivery with tin. *Journal of Geophysical Research: Solid Earth*, *126*(10), e2021JB022026. https://doi.org/10.1029/2021jb022026

Kuwahara, H., Gotou, H., Shinmei, T., Ogawa, N., Yamaguchi, A., Takahata, N., et al. (2017). High pressure experiments on metal-silicate partitioning of chlorine in a magma ocean: Implications for terrestrial chlorine depletion. *Geochemistry, Geophysics, Geosystems*, *18*(11), 3929–3945. https://doi.org/10.1002/2017gc007159

Kuwahara, H., Kagoshima, T., Nakada, R., Ogawa, N., Yamaguchi, A., Sano, Y., & Irifune, T. (2019). Fluorine and chlorine fractionation during magma ocean crystallization: Constraints on the origin of the non-chondritic F/Cl ratio of the Earth. *Earth and Planetary Science Letters*, *520*, 241–249. https://doi.org/10.1016/j.epsl.2019.05.041

Laio, A., Bernard, S., Chiarotti, G. L., Scandolo, S., & Tosatti, E. (2000). Physics of iron at earth's core conditions. *Science*, *287*(5455), 1027–1030. https://doi.org/10.1126/science.287.5455.1027

Laio, A., & Parrinello, M. (2002). Escaping free-energy minima. *Proceedings of the National Academy of Sciences of the United States of America*, *99*(20), 12562–12566. https://doi.org/10.1073/pnas.202427399

Lammer, H., Zerkle, A. L., Gebauer, S., Tosi, N., Noack, L., Scherf, M., et al. (2018). Origin and evolution of the atmospheres of early Venus, Earth and Mars. *Astronomy and Astrophysics Review*, *26*(1), 1–72. https://doi.org/10.1007/s00159-018-0108-y

Layne, G. D., Kent, A. J. R., & Bach, W. (2009). δ^{37}Cl systematics of a backarc spreading system: The Lau Basin. *Geology*, *37*(5), 427–430. https://doi.org/10.1130/g25520a.1

Li, J., & Agee, C. B. (1996). Geochemistry of mantle-core differentiation at high pressure. *Nature*, *381*(6584), 686–689. https://doi.org/10.1038/381686a0

Li, Y., Dasgupta, R., Tsuno, K., Monteleone, B., & Shimizu, N. (2016a). Carbon and sulfur budget of the silicate Earth explained by accretion of differentiated planetary embryos. *Nature Geoscience*, *9*(10), 781–785. https://doi.org/10.1038/ngeo2801

Li, Y., Marty, B., Shcheka, S., Zimmermann, L., & Keppler, H. (2016b). Nitrogen isotope fractionation during terrestrial core-mantle separation. *Geochemical Perspectives Letters*, *2*(2), 138–147. https://doi.org/10.7185/geochemlet.1614

Lodders, K. (2003). Solar system abundances and condensation temperatures of the elements. *The Astrophysical Journal*, *591*(2), 1220–1247. https://doi.org/10.1086/375492

Lodders, K., & Fegley, B. (2023). Solar system abundances and condensation temperatures of the halogens fluorine, chlorine, bromine, and iodine. *Geochemistry*, *83*(1), 125957. https://doi.org/10.1016/j.chemer.2023.125957

Marty, B. (2012). The origins and concentrations of water, carbon, nitrogen and noble gases on Earth. *Earth and Planetary Science Letters*, *313–314*(1), 56–66. https://doi.org/10.1016/j.epsl.2011.10.040

McDonough, W. F., & Sun, S.-S. (1995). The composition of the Earth. *Chemical Geology*, *120*(3–4), 223–253. https://doi.org/10.1016/0009-2541(94)00140-4

Mermin, N. D. (1965). Thermal properties of the inhomogeneous electron gas. *Physics Reviews*, *137*(5A), A1441–A1443. https://doi.org/10.1103/physrev.137.a1441

Morris, J. R., Wang, C. Z., Ho, K. M., & Chan, C. T. (1994). Melting line of aluminum from simulations of coexisting phases. *Physical Review B: Condensed Matter*, *49*(5), 3109–3115. https://doi.org/10.1103/physrevb.49.3109

Mundl-Petermeier, A., Touboul, M., Jackson, M. G., Day, J. M. D., Kurz, M. D., Lekic, V., et al. (2017). Tungsten-182 heterogeneity in modern ocean island basalts. *Science*, *356*(6333), 66–69. https://doi.org/10.1126/science.aal4179

Mungall, J. E., & Brenan, J. M. (2003). Experimental evidence for the chalcophile behavior of the halogens. *The Canadian Mineralogist*, *41*(1), 207–220. https://doi.org/10.2113/gscanmin.41.1.207

Ostanin, S., Alfè, D., Dobson, D., Vočadlo, L., Brodholt, J. P., & Price, G. D. (2006). Ab initio study of the phase separation of argon in molten iron at high pressures. *Geophysical Research Letters*, *33*(6), L06303. https://doi.org/10.1029/2005gl024276

Palme, H., & O'Neill, H. S. C. (2014). Cosmochemical estimates of mantle composition. In *Treatise on geochemistry* (Vol. 3, pp. 1–39). Elsevier.

Palme, H., & Zipfel, J. (2022). The composition of CI chondrites and their contents of chlorine and bromine: Results from instrumental neutron activation analysis. *Meteoritics & Planetary Science*, *57*(2), 317–333. https://doi.org/10.1111/maps.13720

Perdew, J. P., Burke, K., & Ernzerhof, M. (1996). Generalized gradient approximation made simple. *Physical Review Letters*, *77*(18), 3865–3868. https://doi.org/10.1103/physrevlett.77.3865

Porcelli, D., & Halliday, A. N. (2001). The core as a possible source of mantle helium. *Earth and Planetary Science Letters*, *192*(1), 45–56. https://doi.org/10.1016/s0012-821x(01)00418-6

Rubie, D. C., Frost, D. J., Mann, U., Asahara, Y., Nimmo, F., Tsuno, K., et al. (2011). Heterogeneous accretion, composition and core–mantle differentiation of the Earth. *Earth and Planetary Science Letters*, *301*(1–2), 31–42. https://doi.org/10.1016/j.epsl.2010.11.030

Rudge, J. F., Kleine, T., & Bourdon, B. (2010). Broad bounds on Earth's accretion and core formation constrained by geochemical models. *Nature Geoscience*, *3*(6), 439–443. https://doi.org/10.1038/ngeo872

Satish-Kumar, M., So, H., Yoshino, T., Kato, M., & Hiroi, Y. (2011). Experimental determination of carbon isotope fractionation between iron carbide melt and carbon: ^{12}C-enriched carbon in the Earth's core? *Earth and Planetary Science Letters*, *310*(3–4), 340–348. https://doi.org/10.1016/j.epsl.2011.08.008

Self, S., Blake, S., Sharma, K., Widdowson, M., & Sephton, S. (2008). Sulfur and chlorine in late Cretaceous Deccan magmas and eruptive gas release. *Science*, *319*(5870), 1654–1657. https://doi.org/10.1126/science.1152830

Shahar, A., Ziegler, K., Young, E. D., Ricolleau, A., Schauble, E. A., & Fei, Y. (2009). Experimentally determined Si isotope fractionation between silicate and Fe metal and implications for Earth's core formation. *Earth and Planetary Science Letters*, *288*(1–2), 228–234. https://doi.org/10.1016/j.epsl.2009.09.025

Sharp, Z. D., Barnes, J. D., Brearley, A. J., Chaussidon, M., Fischer, T. P., & Kamenetsky, V. S. (2007). Chlorine isotope homogeneity of the mantle, crust and carbonaceous chondrites. *Nature*, *446*(7139), 1062–1065. https://doi.org/10.1038/nature05748

Sharp, Z. D., & Draper, D. S. (2013). The chlorine abundance of Earth: Implications for a habitable planet. *Earth and Planetary Science Letters*, *369–370*, 71–77. https://doi.org/10.1016/j.epsl.2013.03.005

Shi, L., Lu, W., Kagoshima, T., Sano, Y., Gao, Z., Du, Z., et al. (2022). Nitrogen isotope evidence for Earth's heterogeneous accretion of volatiles. *Nature Communications*, *13*(1), 1–15. https://doi.org/10.1038/s41467-022-32516-5

Siebert, J., Badro, J., Antonangeli, D., & Ryerson, F. J. (2012). Metal–silicate partitioning of Ni and Co in a deep magma ocean. *Earth and Planetary Science Letters*, *321–322*, 189–197. https://doi.org/10.1016/j.epsl.2012.01.013

Solomatova, N. V., Caracas, R., & Manning, C. E. (2019). Carbon sequestration during core formation implied by complex carbon polymerization. *Nature Communications*, *10*(1), 1–7. https://doi.org/10.1038/s41467-019-08742-9

Steenstra, E. S., van Haaster, F., van Mulligen, R., Flemetakis, S., Berndt, J., Klemme, S., & van Westrenen, W. (2020). An experimental assessment of the chalcophile behavior of F, Cl, Br and I: Implications for the fate of halogens during planetary accretion and the formation of magmatic ore deposits. *Geochimica et Cosmochimica Acta*, *273*, 275–290. https://doi.org/10.1016/j.gca.2020.01.006

Stevenson, D. J. (1990). Fluid dynamics of core formation. In *Origin of the Earth* (pp. 231–249).

Taniuchi, T., & Tsuchiya, T. (2018). The melting points of MgO up to 4 TPa predicted based on ab initio thermodynamic integration molecular dynamics. *Journal of Physics: Condensed Matter*, *30*(11), 114003. https://doi.org/10.1088/1361-648x/aaac96

Thomas, C. W., & Asimow, P. D. (2013). Direct shock compression experiments on premolten forsterite and progress toward a consistent high-pressure equation of state for CaO-MgO-Al_2O_3-SiO_2-FeO liquids. *Journal of Geophysical Research: Solid Earth*, *118*(11), 5738–5752. https://doi.org/10.1002/jgrb.50374

Thomas, R. W., & Wood, B. J. (2021). The chemical behaviour of chlorine in silicate melts. *Geochimica et Cosmochimica Acta*, *294*(2), 28–42. https://doi.org/10.1016/j.gca.2020.11.018

Turcotte, D., & Schubert, G. (2002). *Geodynamics*. Cambridge University Press.

Usui, Y., & Tsuchiya, T. (2010). Ab initio two-phase molecular dynamics on the melting curve of SiO_2. *Journal of Earth Sciences*, *21*(5), 801–810. https://doi.org/10.1007/s12583-010-0126-9

Wade, J., & Wood, B. J. (2005). Core formation and the oxidation state of the Earth. *Earth and Planetary Science Letters*, *236*(1–2), 78–95. https://doi.org/10.1016/j.epsl.2005.05.017

Wang, W., Li, C. H., Brodholt, J. P., Huang, S., Walter, M. J., Li, M., et al. (2021). Sulfur isotopic signature of Earth established by planetesimal volatile evaporation. *Nature Geoscience*, *14*(11), 806–811. https://doi.org/10.1038/s41561-021-00838-6

Wang, Z., & Becker, H. (2013). Ratios of S, Se and Te in the silicate Earth require a volatile-rich late veneer. *Nature*, *499*(7458), 328–331. https://doi.org/10.1038/nature12285

Waters, E. (2022). *Halogen heterogeneity in the Icelandic mantle source (Ph.D. dissertation)*. University of Manchester.

Widom, M., Huhn, W. P., Maiti, S., & Steurer, W. (2014). Hybrid Monte Carlo/molecular dynamics simulation of a refractory metal high entropy alloy. In *Metallurgical and materials transactions A: Physical metallurgy and materials science* (Vol. 45, pp. 196–200). Springer.

Wood, B. J., Smythe, D. J., & Harrison, T. (2019). The condensation temperatures of the elements: A reappraisal. *American Mineralogist*, *104*(6), 844–856. https://doi.org/10.2138/am-2019-6852ccby

Yang, X., Du, Z., & Li, Y. (2023). Experimental constraints on metal-silicate partitioning of chlorine and implications for planetary core formation. *Geochimica et Cosmochimica Acta*, *355*, 62–74. https://doi.org/10.1016/j.gca.2023.06.017

Yuan, L. (2023). Earth's "missing" chlorine may be in the core [Dataset]. Figshare. https://doi.org/10.6084/m9.figshare.23999010.v2

Yuan, L., & Steinle-Neumann, G. (2020). Strong sequestration of hydrogen into the Earth's core during planetary differentiation. *Geophysical Research Letters*, *47*(15), e2020GL088303. https://doi.org/10.1029/2020gl088303

Yuan, L., & Steinle-Neumann, G. (2021). The helium elemental and isotopic compositions of the Earth's core based on ab initio simulations. *Journal of Geophysical Research: Solid Earth*, *126*(10), e2021JB023106. https://doi.org/10.1029/2021jb023106

Yuan, L., & Steinle-Neumann, G. (2022). Possible control of Earth's boron budget by metallic iron. *Geophysical Research Letters*, *49*(10), e2021GL096923. https://doi.org/10.1029/2021gl096923

Zhang, Y., & Yin, Q. Z. (2012). Carbon and other light element contents in the Earth's core based on first-principles molecular dynamics. *Proceedings of the National Academy of Sciences of the United States of America*, *109*(48), 19579–19583. https://doi.org/10.1073/pnas.1203826109

Zolotov, M. Y., & Mironenko, M. V. (2007). Hydrogen chloride as a source of acid fluids in parent bodies of chondrites. *Lunar and Planetary Science Conference*, *38*(1338), 2340.

References From the Supporting Information

Blanchard, M., Balan, E., & Schauble, E. A. (2017). Equilibrium fractionation of non-traditional isotopes: A molecular modeling perspective. *Reviews in Mineralogy and Geochemistry*, *82*(1), 27–63. https://doi.org/10.2138/rmg.2017.82.2

Kapil, V., Rossi, M., Marsalek, O., Petraglia, R., Litman, Y., Spura, T., et al. (2019). i-PI 2.0: A universal force engine for advanced molecular simulations. *Computer Physics Communications*, *236*, 214–223. https://doi.org/10.1016/j.cpc.2018.09.020

Kowalski, P. M., & Jahn, S. (2011). Prediction of equilibrium Li isotope fractionation between minerals and aqueous solutions at high P and T: An efficient ab initio approach. *Geochimica et Cosmochimica Acta*, *75*(20), 6112–6123. https://doi.org/10.1016/j.gca.2011.07.039

Thompson, A. P., Aktulga, H. M., Berger, R., Bolintineanu, D. S., Brown, W. M., Crozier, P. S., et al. (2022). LAMMPS - A flexible simulation tool for particle-based materials modeling at the atomic, meso, and continuum scales. *Computer Physics Communications*, *271*, 108171. https://doi.org/10.1016/j.cpc.2021.108171

Weeks, J. D., Chandler, D., & Andersen, H. C. (1971). Perturbation theory of the thermodynamic properties of simple liquids. *Journal of Chemical Physics*, *55*(11), 5422–5423. https://doi.org/10.1063/1.1675700

Erratum

The originally published version of this article contained a typographical error. In the first sentence of Section 4, "McDonough and Sun (1995) discussed the possibility that Cl might have been transported to the Earth's center during core format . . ." has been corrected to "McDonough and Sun (1995) discussed the possibility that Cl might have been transported to the Earth's center during core formation . . . ." This may be considered the authoritative version of record.